α1-adrenergic receptors activate Ca^{2+}-permeable cationic channels in prostate cancer epithelial cells

Stephanie Thebault, Morad Roudbaraki, Vadim Sydorenko, Yaroslav Shuba, Loic Lemonnier, Christian Slomianny, Etienne Dewailly, Jean-Louis Bonnal, Brigitte Mauroy, Roman Skryma, and Natalia Prevarskaya

Laboratoire de Physiologie Cellulaire, Institut National de la Santé et de la Recherche Médicale (INSERM) EMI 0228, Villeneuve d'Ascq, France

The prostate gland is a rich source of α1-adrenergic receptors (α1-ARs). α1-AR antagonists are commonly used in the treatment of benign prostatic hyperplasia symptoms, due to their action on smooth muscle cells. However, virtually nothing is known about the role of α1-ARs in epithelial cells. Here, by using two human prostate cancer epithelial (hPCE) cell models — primary cells from resection specimens (primary hPCE cells) and an LNCaP (lymph node carcinoma of the prostate) cell line — we identify an α1A subtype of adrenergic receptor (α1A-AR) and show its functional coupling to plasmalemmal cationic channels via direct diacylglycerol (DAG) gating. In both cell types, agonist-mediated stimulation of α1A-ARs and DAG analogues activated similar cationic membrane currents and Ca^{2+} influx. These currents were sensitive to the α1A-AR antagonists, prazosin and WB4101, and to transient receptor potential (TRP) channel blockers, 2–aminophenyl borate and SK&F 96365. Chronic activation of α1A-ARs enhanced LNCaP cell proliferation, which could be antagonized by α1A-AR and TRP inhibitors. Collectively, our results suggest that α1-ARs play a role in promoting hPCE cell proliferation via TRP channels.

J. Clin. Invest. **111**:1691–1701 (2003). doi:10.1172/JCI200316293.

Introduction

Prostate cancer has the highest incidence of any malignancy and is the second cause of cancer-related deaths in men in industrialized countries (1). Besides metastasis to bone and lymph nodes, the most important reason for prostate cancer mortality is the progression from androgen-dependent to androgen-independent tumors (2). In the case of metastasis, androgen suppression is the leading treatment and currently the most successful. However, as androgen-independent cells are insensitive to this treatment, they continue to grow and prevent cancer regression (3). This insensitivity is a significant problem considering the general aging of the population in the United States and Europe. As hormonal ablation and chemotherapy are not always effective, continuing effort is required to find new targets for therapeutic intervention.

α1-adrenergic receptor (α1-AR) antagonists are already in use for the clinical treatment of benign prostatic hyperplasia, where they act directly on the α1-ARs present in prostatic smooth muscle (4). Recent studies have demonstrated that α1-AR antagonists such as doxazosin and terazosin induce apoptosis in primary human prostate cancer epithelial (hPCE) cells and smooth muscle cells without affecting cellular proliferation (5). While this finding is apparently very promising, the mechanism of apoptosis induction in prostate cancer cells by α-antagonists seems to be α1-AR–independent (5, 6), so whereas prostate epithelial cells seem to express α1-ARs, their functional role in these particular cells has yet to be established.

Among α1-AR subtypes, α1A is believed to be predominant in the fibromuscular stroma of the prostate (7–11). Its stimulation leads principally to the activation of phospholipase C (PLC), ultimately resulting in an increase in intracellular free Ca^{2+} via inositol triphosphate (IP_3) and diacylglycerol (DAG) production (12, 13). Recent studies in vascular smooth muscles have shown that α1-ARs may also activate Ca^{2+}-permeable nonselective cationic channels (14) and that TRPC6 — a member of the transient receptor potential (TRP) channel family originally found in *Drosophila* and then discovered in most mammalian tissues (15) — may be an essential component of these channels (16). Enhanced

Received for publication June 26, 2002, and accepted in revised form April 1, 2003.

Address correspondence to: N. Prevarskaya, Laboratoire de Physiologie Cellulaire, INSERM EMI 0228, Bâtiment SN3, Université des Sciences et Technologies de Lille, 59655 Villeneuve d'Ascq Cedex, France. Phone: 33-3-20-33-60-18; Fax: 33-3-20-43-40-66; E-mail: phycel@univ-lille1.fr.
Y. Shuba's present address is: Bogomoletz Institute of Physiology, Kiev, Ukraine.

Conflict of interest: The authors have declared that no conflict of interest exists.

Nonstandard abbreviations used: α1-adrenergic receptor (α1-AR); human prostate cancer epithelial cell (hPCE cell); phospholipase C (PLC); inositol triphosphate (IP_3); diacylglycerol (DAG); transient receptor potential (TRP); α1A subtype of α1-AR (α1A-AR); lymph node carcinoma of the prostate cells (LNCaP cells); intracellular Ca^{2+} concentration ($[Ca^{2+}]_i$); phenylephrine (Phe); intracellular Ca^{2+} oscillations (osc); 2–aminophenyl borate (2-APB); store-operated Ca^{2+}-channel (SOC); 1-oleoyl-2-acetyl-*sn*-glycerol (OAG); 1,2-dioctanoyl-*sn*-glycerol (DOG); extracellular Ca^{2+} concentration ($[Ca^{2+}]_{out}$); Phe-activated current (I_{Phe}); current reversal potential (E_{rev}).

Ca^{2+} entry due to overexpression of one of the TRPs, TRPC1, has been shown to be linked to the proliferation of human pulmonary myocytes (17). Given that, in general, mitogen-mediated cell growth requires an increase in cytosolic Ca^{2+} concentration (18), these facts highlight the role of TRP channels in maintaining a high intracellular Ca^{2+} concentration during proliferation. However, our data on the expression and physiological roles of TRPs in the prostate are still incomplete.

This study was designed to identify any store-independent mechanisms in α1-AR–activated Ca^{2+} entry in hPCE cells. We show, to our knowledge for the first time, that hPCE cells express the α1A subtype of α1-AR (α1A-AR) and demonstrate that the α1-AR antagonists prazosin and WB4101, as well as SK&F 96365, an inhibitor of receptor-mediated Ca^{2+} entry, inhibit the proliferative effects of α1-AR agonists. Furthermore, our data on the nature of α1-AR–stimulated transmembrane Ca^{2+} entry suggest that it has a substantial store-independent component that is mediated by members of the TRP-channel family.

Methods

Cell cultures. Lymph node carcinoma of the prostate (LNCaP) cells from American Type Culture Collection (Rockville, Maryland, USA) were cultivated in RPMI 1640 medium (BioWhittaker SA, Verviers, Belgium), supplemented with 5 mM L-glutamine (Sigma-Aldrich, L'Isle d'Abeau, France) and 10% FBS (Applera France SA, Courtaboeuf, France). The culture medium also contained 50,000 IU/l penicillin and 50 mg/l streptomycin. Primary hPCE cells were cultivated in KSF medium (Invitrogen SARL, Cergy Pontoise, France) supplemented with 50 μg/ml bovine pituitary extract and 50 ng/ml EGF. Cells were routinely grown in 50-ml flasks (Nunc, Applera France SA) and kept at 37°C in a humidified incubator in an atmosphere of 5% CO_2. For electrophysiology and calcium imagery experiments, the cells were subcultured in Petri dishes (Nunc; Dominique Dutscher SA, Issy-les Moulineaux, France) and used after 3–6 days.

Calcium imaging. Intracellular Ca^{2+} concentration ($[Ca^{2+}]_i$) was measured using Fura-2 (the detailed procedure has been described previously) (19, 20). The extracellular solution contained (in mM): 120 NaCl, 6 KCl, 2 $CaCl_2$, 2 $MgCl_2$, 10 HEPES, and 12 glucose. For Ca^{2+}-free HBSS, $CaCl_2$ was removed and 0.5 mM EGTA was added.

Electrophysiology and solutions. Regular and perforated whole-cell patch-clamp techniques were used for current recording, as detailed elsewhere (21, 22). The extracellular solution contained (in mM): 130 CsCl, 5 KCl, 10 glucose, 2 $CaCl_2$, 2 $MgCl_2$, 10 HEPES, and 20 TEA-OH, adjusted to pH 7.3 with HCl. In the whole-cell experiments, the intracellular solution contained (in mM): 50 CsCl, 90 CsOH, 2 $MgCl_2$, 3 $CaCl_2$ (calculated $[Ca^{2+}]_{free}$ = 280 nM), 5 glucose, 10 HEPES, 4 EGTA, and 2 Na-ATP, adjusted to pH 7.2 with glutamic acid. In the perforated-patch experiments, the intracellular solution contained (in mM): 55 CsCl, 70 Cs_2SO_4, 7 $MgCl_2$, 1 $CaCl_2$, 5 glucose, and 10 HEPES, adjusted to pH 7.2 with CsOH.

For monovalent cation permeability measurements, we omitted KCl from the extracellular solution and replaced it with 135 mM of either NaCl or CsCl. Divalent cation permeability was measured in a solution containing 10 mM $CaCl_2$, $BaCl_2$, or $MgCl_2$ and 125 mM N-methyl-D-glucamine replacing CsCl and KCl. The permeability ratios were calculated on the basis of shifts in reversal potential, using formulas presented in Watanabe et al. (23).

Immunofluorescence staining. The cells were permeabilized in acetone at –20°C for 15 minutes. They were then placed on slides and blocked with 1.2% gelatin in PBS for 30 minutes to avoid nonspecific binding. They were then incubated overnight at 4°C in 100% humidity, together with the primary antibodies for α1A-AR (Santa Cruz Biotechnology Inc., Santa Cruz, California, USA), cytokeratin 18 (NeoMarkers, Fremont, California, USA), and cytokeratin 14 (Chemicon International, Temecula, California, USA). After several washes in 1.2% gelatin in PBS, the slides were incubated at 37°C for 1 hour with the secondary antibodies donkey anti-goat IgG labeled with FITC (Chemicon International) and anti-mouse IgG labeled with Rhodamine Red-X (Jackson ImmunoResearch Laboratories Inc., West Grove, Pennsylvania, USA), then washed in PBS and mounted in Mowiol (Mowiol, Aldrich, France). The sections were observed under a Zeiss Axiophot microscope (Carl Zeiss Inc., Thornwood, New York, USA) equipped with epifluorescence (FITC: excitation, 450–490 nm; emission, 520 nm. Rhodamine Red-X: excitation, 570 nm; emission, 590 nm). Negative controls consisted of the omission of the primary antibody.

Western analysis. Western analysis of protein expression was carried out as previously described (22). Anti–α1A-AR antibody was from Santa Cruz Biotechnology Inc.

RT-PCR analysis. Total RNA from the LNCaP cell line was isolated by the guanidium thiocyanate–phenol-chloroform extraction procedure. After treatment with 0.1 U/μl deoxyribonuclease I (Invitrogen SARL) for 1 hour at 25°C to eliminate genomic DNA, total RNA was reverse transcribed into cDNA as described by Roudbaraki et al. (24). For the PCR reaction, specific sense and antisense primers were selected, based on GenBank TRP sequences, using GeneJockey II (Biosoft, Cambridge, United Kingdom). Primers were synthesized by Invitrogen SARL. Human TRPC1 splice variant TRPC1A–specific sense and antisense primers (GenBank accession no. P19334) were: 5′-TTCCTCTCCATCCTCTTCCTCG-3′ (nucleotides 795–816) and 5′-CATAGTTGTTACGATGAGCAGC-3′ (nucleotides 1,231–1,252). The predicted size of the PCR-amplified product was 457 bp for TRPC1 and 355 bp for the TRPC1A splice variant. Human TRPC3-specific sense and antisense primers (GenBank accession no. U47050) were: 5′-GGAAAAACATTACCTCCACCTTTCA-3′ (nucleotides 2,260–2,284) and 5′-CTCAGTTGCTTGGCTCTTGTCTTCC-3′ (nucleotides 2,619–2,643). The predicted size of the PCR-amplified TRPC3 product was 383 bp.

The primers used for amplification were (a) the 625-bp part of the human TRPC6 coding sequence (GenBank accession no. AJ271066): 5′-GAACTTAGCAATGAACTGGCAGT-3′ (sense, nucleotides 895–917) and 5′-CATATCATGCCTATTACCCAGGA-3′ (antisense, nucleotides 1,499–1,521); and (b) the 477-bp part of human TRPC7 cDNA (GenBank accession no. NM020389): 5′-GTCCGAATGCAAGGAAATCT-3′ (sense, nucleotides 1,356–1,375) and 5′-TGGGTTGTATTTGGCACCTC-3′ (antisense, nucleotides 1,814–1,833).

Each sample was amplified using AmpliTaq Gold DNA Polymerase (Applied Biosystems, Foster City, California, USA) in an automated thermal cycler (GeneAmp 2400; Applied Biosystems). DNA amplification conditions included an initial 7-minute denaturation step at 95°C (which also activated the AmpliTaq Gold) and 40 cycles of 30 seconds at 95°C, 30 seconds at 58°C, 40 seconds at 72°C, and a final elongation of 7 minutes at 72°C. The RT-PCR samples were electrophoresed on a 1.5% agarose gel and stained with ethidium bromide (0.5 μg/ml), then photographed under UV light. In order to study band identity, the RT-PCR products were subjected to restriction enzyme analysis.

Proliferation assays. The CellTiter 96 AQueous Non-Radioactive Cell Proliferation Assay (Promega Corp., Madison, Wisconsin, USA) was used to determine the number of viable cells in proliferation assays. This commercial assay is composed of MTS (inner salt) and PMS (an electron coupling reagent). MTS is bioreduced by cells into a formazan that is soluble in the tissue culture medium. The absorbance of the formazan at 490 nm is measured directly from 96-well assay plates. The quantity of formazan produced, measured by the amount of 490 nm absorbance, is directly proportional to the number of living cells in the culture. The Dunnet test was used for statistical analyses.

Data analysis. Each experiment was repeated several times and the results were expressed as mean ± SEM where appropriate. The data were analyzed and graphs were plotted using Origin 5.0 software (Microcal Software Inc., Northampton, Massachusetts, USA). Characteristic times of membrane current or $[Ca^{2+}]_i$ response to any intervention were determined as follows. The time intervals from the onset of the intervention until the current or $[Ca^{2+}]_i$ reached $0.05(A_{max} - A_{base})$ and $0.95(A_{max} - A_{base})$ were considered as latency and time-to-peak response periods, respectively, where A_{base} is the baseline signal amplitude before the intervention and A_{max} is the maximal signal amplitude. The time interval between $0.05(A_{max} - A_{base})$ and $0.95(A_{max} - A_{base})$ was considered to be the response development time.

Results

α1A-AR protein expression in hPCE cells. α1A-ARs are primarily distributed in the fibromuscular stroma of the prostate. To demonstrate the expression of α1-ARs in a primary culture of hPCE cells and in the androgen-dependent LNCaP cell line, we used an immunodetection strategy with a specific antibody for α1A-AR, considered to be the dominant subtype in the prostate. Figure 1 shows that both primary hPCE cells and LNCaP cells express α1A-AR. With FITC-labeled secondary antibody alone, no immunoreactivity was detected in either cell type in response to treatment (data not shown).

Evidence of functional α1-AR in hPCE cells. Having demonstrated the presence of α1A-AR in hPCE cells, we investigated whether stimulation of this receptor affected intracellular Ca^{2+} homeostasis. Figure 2 shows that applying the α1-specific agonist phenylephrine (Phe, 10 μM) to primary hPCE cells elicited intracellular Ca^{2+} oscillations (osc), which occurred only during agonist application, with an average frequency of 1 osc/8.4 ± 0.6 min and an average duration of 2.6 ± 0.2 min (Figure 2a, n = 17). These oscillations were suppressed by SK&F 96365, a conventional blocker of receptor-operated Ca^{2+} entry (25) (10 μM, Figure 2b, n = 9), suggesting that Ca^{2+} entry is essential to the generation of these oscillations. Exposure of LNCaP cells to 10 μM Phe induced a slow, gradual increase in $[Ca^{2+}]_i$, within 29.0 ± 1.8 min, followed only by minor oscillations around the $[Ca^{2+}]_i$ plateau (Figure 2c, n = 37), which, however, was also sensitive to SK&F 96365 (see Figure 2e). This dramatic difference in $[Ca^{2+}]_i$ signal kinetics in response to Phe between the primary hPCE cells and LNCaP cells sug-

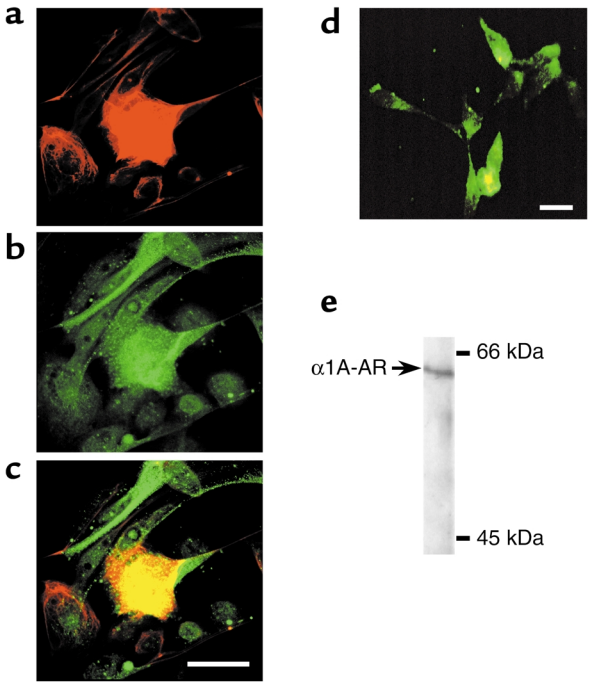

Figure 1
α1A-AR protein expression in hPCE cells. (**a**–**c**) Epifluorescence images representing double labeling of the primary culture of hPCE cells with anti–cytokeratin 14 antibody that selectively stains epithelial cells (red in **a**) and with goat anti–α1A-AR antibody (green in **b**), resulting in an orange interference color (**c**). (**d**) Staining of LNCaP cells with goat anti–α1A-AR antibody. (**e**) Representative Western blot analysis of α1A-AR in LNCaP cells with goat anti–α1A-AR polyclonal antibody (see Methods for details). Each experiment was repeated several times.

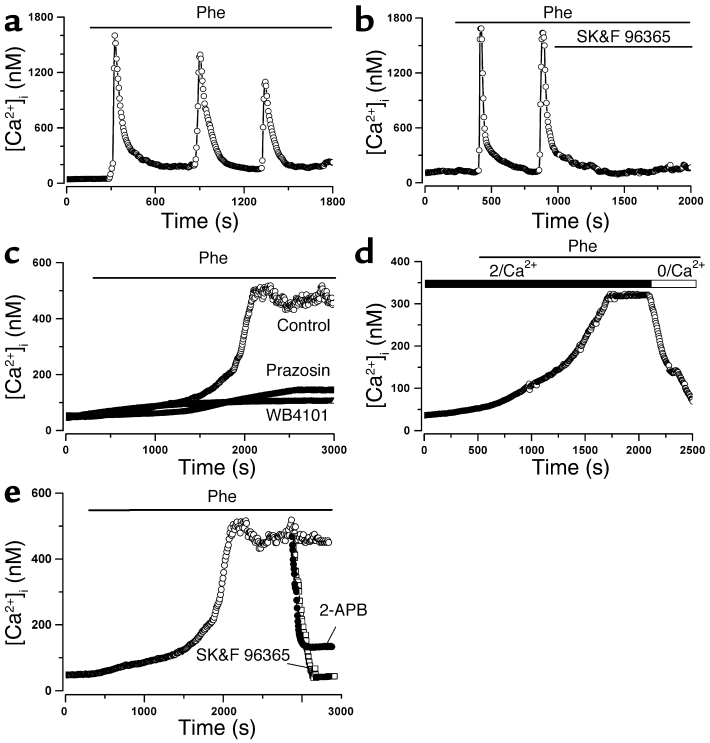

Figure 2
α1A-AR agonist–evoked Ca^{2+} signaling in human prostate epithelial cells. (**a** and **b**) Changes in $[Ca^{2+}]_i$ in representative primary human prostate epithelial cells in response to Phe (10 μM, *n* = 17) (**a**) alone and (**b**) in combination with SK&F 96365 (10 μM, *n* = 9). (**c**) Phe-evoked changes in $[Ca^{2+}]_i$ in representative LNCaP cells under control conditions (*n* = 37) and in the presence of the α1-AR antagonists prazosin (*n* = 31) or WB4101 (*n* = 33) (both at 1 μM). (**d**) Phe-evoked $[Ca^{2+}]_i$ increase in LNCaP cells at 2 mM extracellular Ca2+ ($2/Ca^{2+}$) and the decrease on removal of extracellular Ca^{2+} ($0/Ca^{2+}$) (*n* = 29). (**e**) Blockade of Phe-evoked $[Ca^{2+}]_i$ increase in two representative LNCaP cells by SK&F 96365 (10 μM, *n* = 10) and 2-APB (100 μM, *n* = 10). $[Ca^{2+}]_i$ signals were measured on Fura-2–loaded cells; all interventions in each panel are marked by horizontal bars.

gests quite different modes of Ca^{2+} entry, release, and uptake in the two cell types. As LNCaP cells were much more accessible for experimental use than primary hPCE cells, most of the experiments reported in this study used LNCaP cells.

The Phe-induced $[Ca^{2+}]_i$ increase in LNCaP cells was completely inhibited by competitive α1A-AR antagonists such as prazosin and WB4101 (both at 1 μM). In addition, this validated the involvement of α1-ARs (Figure 2c, *n* = 31 and *n* = 33 respectively). To determine the origin of the agonist-evoked $[Ca^{2+}]_i$ rise in LNCaP cells, we used extracellular media with varying Ca^{2+} content. Figure 2d (*n* = 9) shows that removal of extracellular Ca^{2+} during the plateau of the Phe-evoked $[Ca^{2+}]_i$ increase caused a sharp decline in $[Ca^{2+}]_i$, suggesting that virtually all of the Ca^{2+} entered the cell from extracellular space. Moreover, in Ca^{2+}-free media, Phe did not induce any $[Ca^{2+}]_i$ increase (data not shown). Similar $[Ca^{2+}]_i$ responses were caused in LNCaP cells by the nonspecific adrenergic agonist epinephrine (see Figure 4a, *n* = 31), suggesting that β-ARs play, at most, a negligible role. This would therefore justify the interchangeable usage of the two agonists.

To further validate the involvement of plasmalemmal Ca^{2+}-permeable channels in the α1-AR–stimulated Ca^{2+} influx in LNCaP cells, we tested the ability of SK&F 96365 and 2–aminophenyl borate (2-APB), an IP_3 receptor and a store-operated Ca^{2+}-channel (SOC) inhibitor (25, 26), to interfere with the effect of Phe on Ca^{2+} homeostasis. Figure 2e shows that both drugs at their typically used concentrations (10 μM SK&F 96365, *n* = 10 and 100 μM 2-APB, *n* = 10) effectively blocked Phe-induced Ca^{2+} entry, although SK&F 96365 appeared to be slightly more potent, inhibiting virtually 100% of the response, compared with about 80% for 2-APB (Figure 2e).

DAG partially mimics the effects of α1-AR stimulation. By acting via α1-ARs, Phe stimulates the entire PLC-catalyzed inositol phospholipid–breakdown signaling pathway, which eventually results in the activation of IP_3 store–dependent and store–independent Ca^{2+} entry. The latter would, in all probability, be carried via members of the short subfamily of TRP channels (15), including TRPC1 (27), TRPC3 (27–29), TRPC6 (16, 29, 30), and TRPC7 (31). All of the latter can be directly activated by DAG (a second byproduct of PLC-catalyzed phospholipid turnover) via a mechanism independent of PKC.

To dissect the store-independent component of α1-AR agonist–stimulated Ca^{2+} influx into LNCaP cells and assess the role of DAG in this influx, we used two membrane-permeable DAG analogues, a 1-oleoyl-2-acetyl-*sn*-glycerol (OAG) and a 1,2-dioctanoyl-*sn*-glycerol (DOG). The application of OAG (100 μM) to LNCaP cells elicited $[Ca^{2+}]_i$ oscillations (which occurred only during OAG application, with an average frequency of 1 osc/9.8 ± 1 min and an average duration of 2.6 ± 0.2 min; Figure 3a, *n* = 37). These oscillations were very similar to those observed in primary hPCE cells in response to Phe (see Figure 2a). Furthermore, they were dependent on extracellular calcium concentration ($[Ca^{2+}]_{out}$,) completely vanishing in a nominally Ca^{2+}-free extracellular solution (Figure 3b, *n* = 45), and were completely suppressed by either SK&F 96365 (10 μM, Figure 3c, *n* = 15) or 2-APB (100 μM, Figure 3d, *n* = 24). The application of another DAG analogue, DOG (100 μM), to LNCaP cells produced only a transient increase in $[Ca^{2+}]_i$ (Figure 3e,

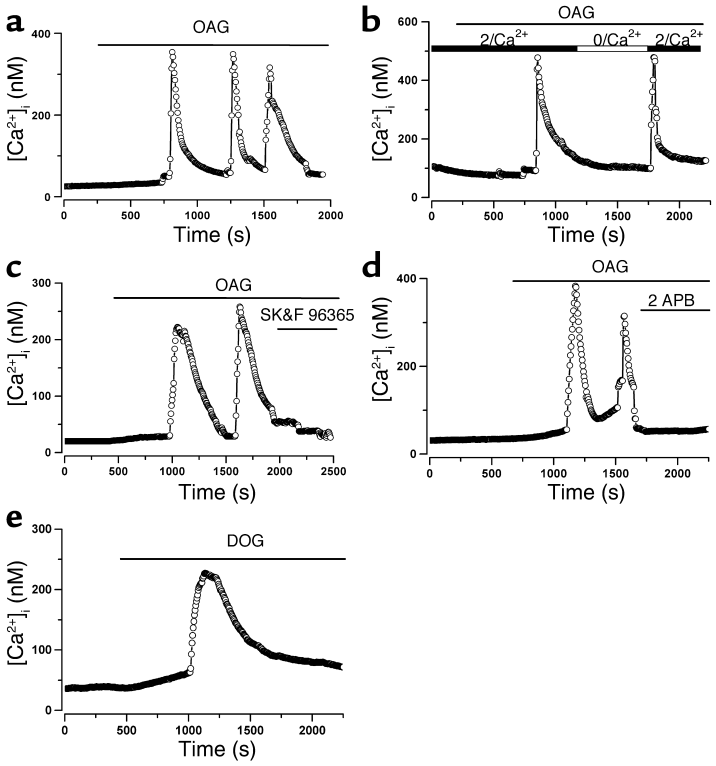

Figure 3
Membrane-permeable DAG analogues induce $[Ca^{2+}]_i$ signaling in LNCaP cells. (**a**) $[Ca^{2+}]_i$ oscillations in a representative LNCaP cell evoked by the membrane-permeable DAG analogue OAG (100 μM, *n* = 37). (**b**) OAG-evoked $[Ca^{2+}]_i$ oscillations in a LNCaP cell disappear in nominally Ca^{2+}-free medium (0/Ca^{2+}, *n* = 45). (**c** and **d**) Coapplications of cationic channel blockers SK&F 96365 (10 μM, *n* = 15) (**c**) and 2-APB (100 μM, *n* = 24) (**d**) suppress OAG-evoked $[Ca^{2+}]_i$ oscillations in LNCaP cells. (**e**) Representative transient $[Ca^{2+}]_i$ increase induced in a LNCaP cell by another membrane-permeable DAG analogue, DOG (100 μM, *n* = 23). $[Ca^{2+}]_i$ signals were measured on Fura-2–loaded cells; all interventions on each panel are marked by horizontal bars.

n = 23), which was, however, dependent on $[Ca^{2+}]_{out}$ as OAG-induced oscillations. Moreover these oscillations were sensitive to SK&F 96365 and 2-APB (data not shown). Thus, the experiments with DAG analogues indicate that transmembrane Ca^{2+} entry into LNCaP cells bypassing α1-AR stimulation can be activated by using one of its downstream products that does not affect IP_3-dependent Ca^{2+} stores. In addition, this product probably targets the subset of membrane channels that contribute to overall Ca^{2+} entry, which is associated with α1-AR stimulation.

In order to prove the dependence of α1-AR agonist–evoked Ca^{2+} entry on the signaling cascade triggered by PLC-catalyzed phospholipid turnover, we used the PLC inhibitor U73122 and its inactive analogue U73343 (32, 33). Figure 4a shows that pretreatment of LNCaP cells with 10 μM U73122 (*n* = 12) for 15 minutes completely prevented the epinephrine-induced $[Ca^{2+}]_i$ increase, whereas U73343 exerted no inhibitory effect under equivalent conditions (*n* = 19). We also investigated whether PKC activation contributed to the effect of DAG analogues on Ca^{2+} entry into LNCaP cells. LNCaP cells were pretreated for 30 minutes with one of the following PKC inhibitors: staurosporine (1 μM, *n* = 17), *bis*-indolylmaleimide I (500 nM, *n* = 33), or GÖ6976 (50 nM, *n* = 13) for 30 minutes. Cells were then exposed to 100 μM OAG. Figure 4b shows that this pretreatment did not interfere with the ability of OAG to induce $[Ca^{2+}]_i$ oscillations. Indeed, the average frequency and duration of the OAG-induced oscilla-

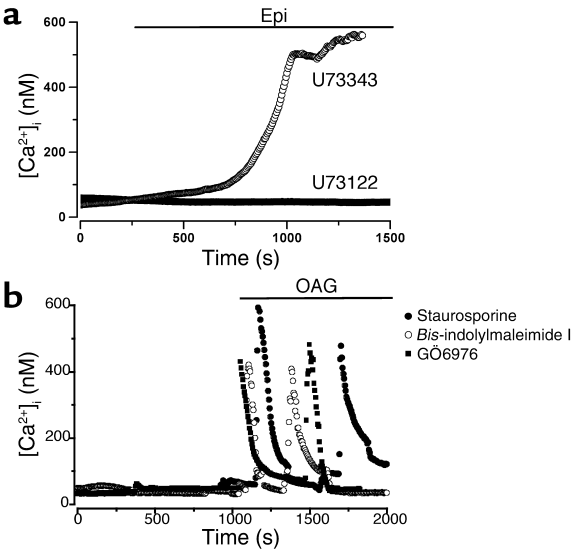

Figure 4
α1-AR–mediated $[Ca^{2+}]_i$ signaling in LNCaP cells is PLC- but not PKC-dependent. (**a**) Two superimposed representative $[Ca^{2+}]_i$ signals evoked by epinephrine (Epi) (1 μM) in the presence of the PLCβ inhibitor U73122 (10 μM, *n* = 12, no increase in $[Ca^{2+}]_i$) and its inactive analogue U73343 (10 μM, *n* = 19). (**b**) Three superimposed representative $[Ca^{2+}]_i$ transients evoked by OAG (100 μM) in LNCaP cells pretreated for 30 minutes with one of the following PKC inhibitors: staurosporine (1 μM, *n* = 17), *bis*-indolylmaleimide I (500 nM, *n* = 33), or GÖ6976 (50 nM, *n* = 13), demonstrating the ineffectiveness of PKC inhibition. $[Ca^{2+}]_i$ signals were measured in Fura-2–loaded cells; all interventions on each panel are marked by horizontal bars.

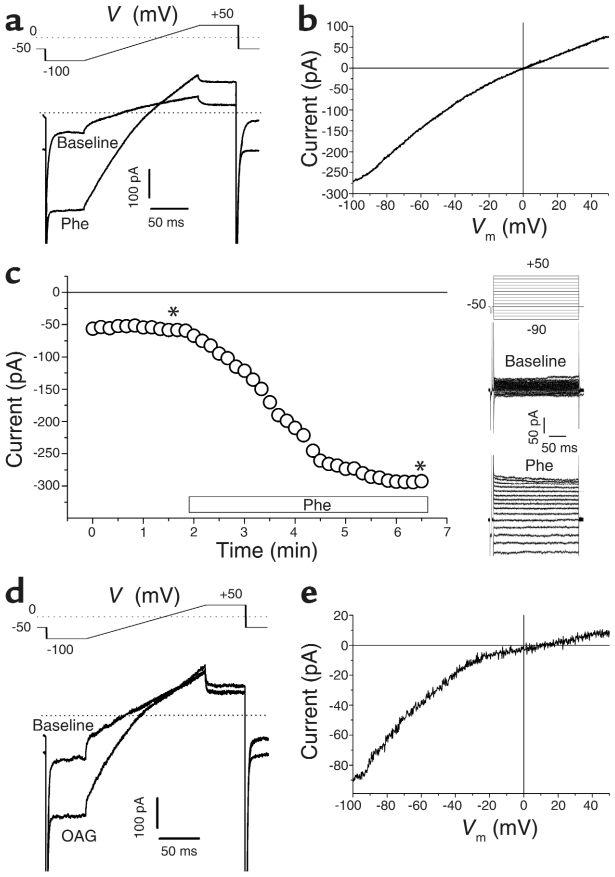

Figure 5
Phe and OAG activate cationic membrane current in LNCaP cells. (**a** and **b**) Superimposed recordings of the baseline current and current in the presence of Phe (50 μM) in representative LNCaP cells (**a**; pulse protocol is shown above the records) and *I-V* relationship of Phe-induced current derived from ramp portions of the recordings (**b**). (**c**) Phe-induced current (measured at –100 mV). Each trace shows mean ± SEM current density in response to Phe application (horizontal bar) (n = 9). The right-hand panel presents original baseline (top) and Phe-induced (bottom) currents recorded at the times marked by asterisks (pulse protocol is shown above the baseline currents). Superimposed recordings of the baseline current and current in the presence of Phe (50 μM) in representative LNCaP cell exposed to OAG (100 μM) (**d**) and corresponding *I-V* relationship (**e**).

tions in the presence of PKC inhibitors (1 osc/9.5 ± 0.8 min, data not shown) was similar to that estimated in the absence of PKC inhibitors (1 osc/9.8 ± 1.0 min). These results rule out PKC involvement in $[Ca^{2+}]_i$ oscillations and strongly suggest that OAG may act directly on the channels, underpinning the notion of agonist-evoked Ca^{2+} influx into LNCaP cells.

α1-AR stimulation activates an inwardly rectifying cationic current similar to that induced by OAG. Fluorescent $[Ca^{2+}]_i$ measurements provide only a rough estimate of the Ca^{2+} influx, as the resulting $[Ca^{2+}]_i$ signal is strongly affected by intracellular Ca^{2+} handling mechanisms. To demonstrate directly that α1-AR stimulation translates into the activation of store-independent membrane channels, we carried out whole-cell patch-clamp recordings of Phe-induced membrane currents. Experiments were performed on LNCaP cells under conditions that ensured both the effective suppression of the voltage-dependent K^+ current characteristic of these cells (21) and the prevention of passive intracellular Ca^{2+} store depletion that could lead to the activation of SOCs (i.e., high $[Ca^{2+}]_{free}$ in the pipette solution). Changes in the membrane current in response to voltage-clamp pulses were continuously monitored. These pulses included a linear-ramp portion connecting two steady levels of –100 mV and +50 mV applied every 10 seconds (Figure 5a). Under our experimental conditions, these pulses (Figure 5a), as well as regular stepwise pulses to different membrane potentials (V_m, Figure 5b), elicited only a small background current that was considered a baseline for further examinations. Phe application (50 μM) caused the development of the current, which reached its full amplitude in about 4.0 ± 0.8 min (Figure 5b) and showed no signs of voltage- or time-dependent gating (Figure 5, a and b). The average density of Phe-evoked current was 23.0 ± 1.8 pA/pF at V_m = –100 mV (n = 9). The *I-V* relationship derived from the ramp portions of the currents, which displayed quite prominent inward rectification (Figure 5a). Phe-induced current was reversibly inhibited by SK&F 96365 (22 ± 5% at 10 μM and V_m = –100 mV) and 2-APB (58 ± 6% at 100 μM and V_m = –100 mV) (data not shown), suggesting that it was transferred via α1-AR–coupled cationic membrane channels.

In order to study the development of Phe-activated current (I_{Phe}) cationic current under more physiological experimental conditions than those of the conventional whole-cell configuration, we used the perforated-patch recording technique. Figure 6 shows the time course of I_{Phe} development. In all the perforated-patch experiments (n = 7), the latency before I_{Phe} activation (calculated as described in Methods) was prolonged, at 6.4 ± 0.5 min, compared with 0.2 ± 0.1 min in the conventional whole-cell configuration. However, the response development time and average density of I_{Phe} were similar in

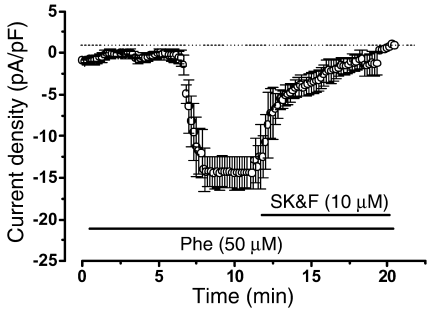

Figure 6
Combined perforated-patch recording of the Phe-evoked inwardly rectifying cationic current at a holding potential of –100 mV (see Methods). The data are mean ± SEM for seven cells. The horizontal black bars indicate the applications of 50 μM Phe and 10 μM SK&F 96365.

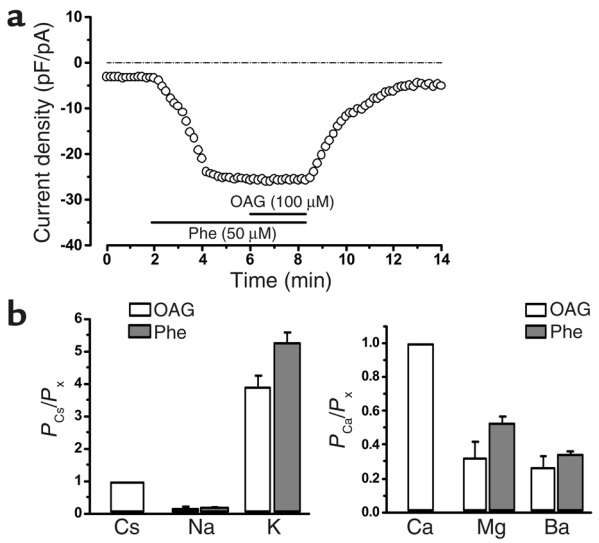

Figure 7
Phe-activated channels are similar to those activated by OAG. Selectivity properties of OAG- and Phe-induced current in LNCaP cells. (**a**) Cumulative data (mean ± SEM) for OAG (n = 4 cells) and Phe (n = 7 cells) for monovalent (left panel) and divalent (right panel) ion selectivity for Phe- and OAG-induced current. Permeability to Cs^+ (P_{Cs^+}/P_X) and Ca^{2+} ($P_{Ca^{2+}}/P_X$) was calculated as indicated in Methods. (**b**) Time course of an inwardly rectifying current in representative LNCaP cells (at V_m –100 mV) in response to 50 μM Phe alone and after coapplication of 100 μM OAG (n = 4). All interventions on each panel are marked by horizontal bars.

both perforated (1.45 ± 0.5 min and 15.0 ± 1.9 pA/pF at V_m = –100 mV, Figure 6) and conventional whole-cell configurations (2.6 ± 0.5 min and 23.0 ± 2.7 pA/pF at V_m = –100 mV, Figure 5b). Phe-induced current was also reversibly inhibited by SK&F 96365 (10 μM, n = 4, Figure 6) under perforated-patch conditions.

Current with similar properties to that elicited by Phe could also be induced by the membrane-permeable DAG analogue OAG (100 μM, Figure 5, d and e). This is consistent with the hypothesis that I_{Phe} is directly activated via the DAG branch of the receptor-bound PLC-catalyzed inositol phospholipid–breakdown signaling pathway after stimulation of α1-ARs. The average density of OAG-induced current was 23.0 ± 2.8 pA/pF at V_m = –100 mV (n = 7), with a reversal potential of around 0 mV.

In order to quantify the relative permeability of monovalent cations through α1-AR agonist and OAG-activated membrane channels, we replaced all and K^+ in the divalent cation–free extracellular solution with equimolar amounts of Na^+ and Cs^+. We then measured the shifts in current reversal potential (E_{rev}). On the basis of the E_{rev} shifts, the following order of relative permeability was deduced for Phe (n = 7): P_K (5.3) > P_{Cs} (1.0) > P_{Na} (0.2) and OAG (n = 4): P_K (3.9) > P_{Cs} (1.0) > P_{Na} (0.2) (Figure 7b).

Given that P_{Cs+} is higher than P_{Na+} that Cs^+ is also able to carry far more current than Na^+, Cs^+ was used as a major charge carrier for further characterization of α1-AR–coupled cationic channels, unless otherwise specified. Cs^+ was used instead of K^+ to ensure the reliable suppression of any contribution from voltage-gated K^+ channels. We were also interested in discovering whether Phe- and OAG-activated membrane channels were permeable to divalent cations, particularly Ca^{2+}. To check the possible permeation of various divalent cations, we formulated an extracellular solution in which most of the Cs^+ was replaced with nonpermeating N-methyl-d-glucamine and raised the concentration of the tested divalent cation (Ca^{2+}, Mg^{2+}, or Ba^{2+}) to 10 mM (see Methods). Phe was still able to induce current above the baseline level in the presence of all of the ions tested, suggesting its passage through the channel. Tabulation of the shifts in reversal potential relative to Ca^{2+} yielded the following order of relative permeability for Phe (n = 7): P_{Ca} (1.0) > P_{Mg} (0.5) > P_{Ba} (0.3) and for OAG (n = 4): P_{Ca} (1.0) > P_{Mg} (0.3) > P_{Ba} (0.3) (Figure 7b). Following the removal of extracellular Ca^{2+}, the amplitude of the OAG-induced current at –100 mV decreased by about 20% (data not shown). This suggested that Ca^{2+} is an essential component of the overall cationic current, thus contributing to the fluorometrically measured Phe- and OAG-induced increase in $[Ca^{2+}]_i$. The electrophysiological properties of the OAG-induced current are similar to those of the Phe-induced current, i.e., voltage dependence (inward-

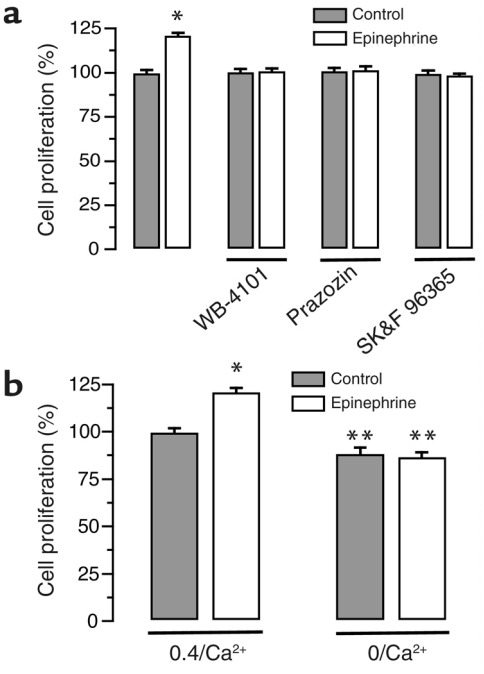

Figure 8
The effects of α1A-AR stimulation on LNCaP cell proliferation. (**a**) Bar graph showing the change in cell density following 48 hours of incubation under control conditions (gray bars) and in the presence of epinephrine (0.5 μM, white bars), alone or in combination with the α1A-AR antagonists WB-4101 (1 μM) or prazosin (1 μM), or the cationic channel blocker SK&F 96365 (10 μM). (**b**) Epinephrine stimulated cell growth in the presence of extracellular Ca^{2+} (0.4 mM, 0.4/Ca^{2+}), but not in its absence (0/Ca^{2+}), although Ca^{2+}-free medium alone inhibits cell growth. *P < 0.05. **P < 0.01. Bars represent mean ± SEM, n = 8.

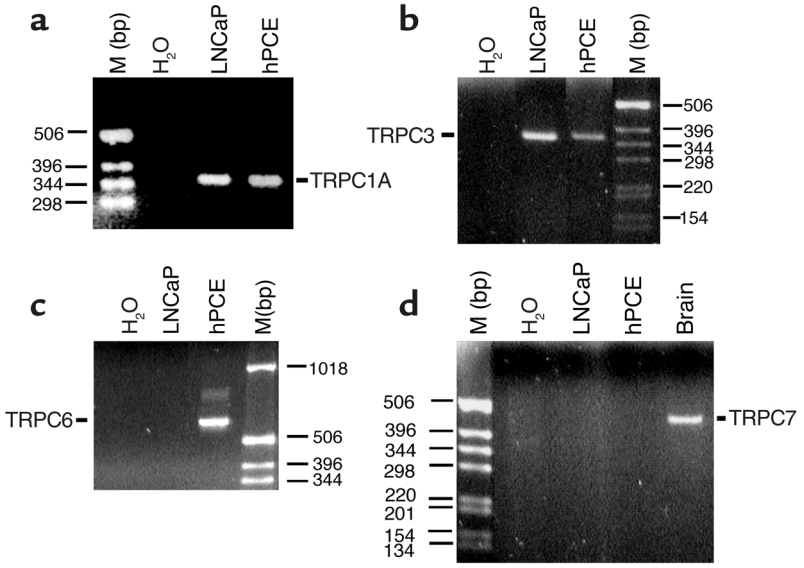

Figure 9
Expression of DAG-gated TRPs in primary hPCE cells and LNCaP cells. RT-PCR analysis of the expression of human TRPC1A (**a**), TRPC3 (**b**), TRPC6 (**c**), and TRPC7 (**d**) transcripts in hPCE and LNCaP cells. The expression products were obtained using the primers described in Methods. Brain tissue was used as a positive control for TRPC7 detection. M, DNA ladder.

ly rectifying *I-V*), current density, reversal potential, and ion permeability sequence.

To verify the hypothesis that DAG may be actively involved in Phe-induced cationic current, we investigated the additional application of both agonists, Phe and the membrane-permeable DAG analogue OAG. Figure 7a shows that, in LNCaP cells, the application of Phe elicited a cell membrane current, I_{Phe}, and that the application of OAG at maximum I_{Phe} (during maximal Phe-induced response) had no additional effect (n = 4). Similarly, the application of OAG elicited a current indistinguishable from that evoked by Phe, and the application of Phe during maximal OAG-induced response had no additional effect (data not shown). The current densities (26.5 ± 2.1 pA/pF and 25.0 ± 2.5 pA/pF at V_m = –100 mV, respectively) and reversal potential (~0 mV) were similar in the presence of both agonists. These data strongly suggest that the α1-AR agonist targets the same channels as OAG. Moreover, pretreatment with PKC inhibitors such as staurosporine modified neither OAG-induced (n = 4) nor Phe-induced (n = 6) currents.

α1-ARs and LNCaP cell proliferation. To determine whether α1-ARs are involved in LNCaP cell proliferation, we examined the effect of culturing cells in medium supplemented with the agonist epinephrine, either alone, in combination with one of the two α1-AR antagonists (prazosin or WB4101), or with a cationic channel inhibitor, SK&F 96365. Two days of treatment with 1 μM epinephrine resulted in about 25% cell growth promotion, which was α1-AR–specific, as it was completely abolished by the competitive α1-AR antagonists prazosin and WB4101 (Figure 8a). The proliferative action of α1-AR stimulation was apparently mediated by Ca^{2+} influx through plasmalemmal cationic channels, as coincubation of the cells with 10 μM SK&F 96365 inhibited epinephrine-evoked proliferation (Figure 8a). Interestingly, 10 μM SK&F 96365 alone had no effect on LNCaP cell viability, although a preferential inhibitor of IP_3 receptors and SOCs, 2-APB (100 μM), was able to suppress cell proliferation (data not shown).

To demonstrate that Ca^{2+} influx was required for α1-AR–stimulated proliferation of LNCaP cells, we repeated the experiments with epinephrine (1 μM) incubation at various concentrations of extracellular Ca^{2+}. Figure 8b shows that at 0.4 mM $[Ca^{2+}]_{out}$, epinephrine-induced cell proliferation was similar to that observed at the normal $[Ca^{2+}]_{out}$ of 2 mM (see Figure 8a). However, epinephrine lost its ability to stimulate cell proliferation in nominally Ca^{2+}-free extracellular medium, which itself inhibited cell growth (Figure 8b).

Collectively, these results suggest that α1-ARs play an essential role in promoting hPCE cell proliferation and highlight the significance in this process of α1-AR–stimulated transmembrane Ca^{2+} influx via plasmalemmal cationic channels.

Expression of receptor-operated TRP channels in hPCE cells. As previously mentioned, four members of the short subfamily of TRP channels, TRPC1, TRPC3, TRPC6, and TRPC7 (15), are the most implicated in the receptor-operated, store-independent Ca^{2+} entry linked to the inositol phospholipid–breakdown signaling cascade. We therefore attempted to identify the α1-AR–coupled cationic channel in hPCE cells. This was done using RT-PCR analysis to determine the expression of mRNA specific to the human isoforms of these TRPs in primary hPCE and LNCaP cells. Figure 9 shows that the transcripts for the TRPC1A splice variant (Figure 9a) and TRPC3 (Figure 9b) were abundantly expressed in the LNCaP cell line, whereas TRPC6 (Figure 9c) and TRPC7 (Figure 9d) were undetectable. In primary hPCE cells the situation was somewhat different: these cells expressed TRPC1A (Figure 9a) and TRPC6 (Figure 9c) strongly, TRPC3 weakly (Figure 9d), and TRPC7 not at all (Figure 9d). However, it is premature to identify exactly which TRPs contribute to the α1-AR–stim-

ulated store-independent Ca^{2+} entry in the two cell types and in what proportion simply on the basis of expression patterns.

Discussion

This study presents, we believe for the first time, evidence of the role of α1-ARs in transmembrane Ca^{2+} signaling in hPCE cells. It also demonstrates the involvement of this signaling in the proliferation of these cells. Furthermore, it shows that the α1-AR subtype expressed in hPCE cells is α1A, and that α1A-AR–stimulated transmembrane Ca^{2+} influx contains an essential cationic store–independent component, which is probably provided by the members of the TRP-channel family.

α1-ARs in the prostate and cell proliferation. The role of α1-ARs in agonist-stimulated proliferation has mainly been demonstrated for smooth muscle myocytes (34, 35), although there is evidence that these receptors may participate in the promotion of proliferation of other cell types as well (36). Moreover, recent studies demonstrate that some of the immediate targets for α1-AR–mediated regulation, at least in smooth muscle cells, are Ca^{2+}-permeable cationic channels in the TRP-channel family (16). These works have shown that these channels can be activated directly by DAG, one of the products of the α1-AR–coupled inositol phospholipid hydrolysis signaling cascade (29, 30). Enhanced Ca^{2+} influx mediated by overexpression of the TRP-channel TRPC1 is directly involved in the proliferation of vascular smooth muscle cells (17).

Four subtypes of α1-ARs (α1A, α1B, α1C, and α1L) have been identified in human prostate cells (7–11). These receptors are mostly localized in the fibromuscular stroma, where they mediate the contraction of prostate smooth muscle (8). While the role of α1-ARs in maintaining the contractile properties of the prostate has been intensively investigated, and has even received widespread recognition in the clinical treatment of benign prostatic hyperplasia, the representation and function of these receptors in the glandular epithelium have yet to be determined. At the same, there is growing evidence that α1-ARs support the direct mitogenic effect of catecholamines on prostate growth (37).

Our study is the first to provide direct evidence that both primary hPCE cells and LNCaP epithelial cells express the α1A subtype of α1-ARs and that this receptor is functionally coupled to transmembrane Ca^{2+} entry via the PLC-catalyzed inositol phospholipid–breakdown signaling pathway, presumably through activation of channels in the TRP family. This Ca^{2+} entry seems to be a dominant source of the Ca^{2+} required to promote the proliferation of LNCaP cells. The specificity of α1-AR agonist–induced proliferation is proven by its complete suppression by α1-AR inhibitors, such as prazosin and WB4101. Moreover, α1-AR agonist–stimulated proliferation of LNCaP cells was also inhibited by the endogenous cationic channel and the TRP channel blockers 2-APB and SK&F 96365, suggesting that these channels are involved in the proliferative effect of α1-AR agonists.

Candidates for α1-AR–coupled channels in prostate cancer epithelial cells. As α1-ARs act via PLC-catalyzed production of two second-messengers, IP_3 and DAG (12), two mechanisms are probably involved in Ca^{2+} entry in response to the stimulation of these receptors by agonists. The first is related to the IP_3-evoked depletion of intracellular Ca^{2+} stores and the subsequent activation of plasmalemmal SOCs, also thought to belong to the TRP-channel family (15). The second, however, is related to the direct DAG-mediated activation of other TRP members (15, 29).

Our $[Ca^{2+}]_i$ measurements, together with previous work showing the presence of SOC-mediated Ca^{2+} entry into LNCaP cells (22, 30), suggest that both mechanisms are activated in response to α1-AR stimulation. Furthermore, the α1-AR agonist Phe, which activates the entire inositol phospholipid–breakdown signaling cascade, and membrane-permeable DAG analogues, which affect only the DAG-dependent branch of this cascade (i.e., PKC activation and direct action on TRP channels), produced kinetically distinct $[Ca^{2+}]_i$ signals in LNCaP cells.

Both signals, however, were dependent on $[Ca^{2+}]_{out}$ and were sensitive to SK&F 96365. Thus, $[Ca^{2+}]_i$ measurements using DAG derivatives, and even more significantly, direct patch-clamp measurements of Phe- and OAG-induced membrane currents, unequivocally demonstrated that this subset of Ca^{2+}-permeable membrane channels, activated independently of store depletion, were present in LNCaP cells. Indeed, this agonist-induced Ca^{2+} entry and the corresponding currents were measured using Fura-2 Ca^{2+} imaging, conventional whole-cell patch-clamping, and perforated-patch techniques. The average density and response development time of I_{Phe} were similar in both perforated and conventional whole-cell configurations. However, a longer (6-minute) latency period before I_{Phe} activation was observed in the perforated-patch recordings. This prolonged latency may be explained by the wash-out of some intracellular factors in conventional whole-cell configuration, such as delayers or channel activation modulators. Indeed, we had previously verified the rate of intracellular perfusion in LNCaP cells (38): it took about 3–4 minutes to replace half the cell cytoplasm solution with pipette solution. In the Fura-2 experiments, the $[Ca^{2+}]_i$ response latency was even more prolonged (at least 20 minutes). Although the Ca^{2+} component was essential to the overall cationic current measured by patch-clamp recordings, therefore allowing Ca^{2+} ions to enter the cell, we have not yet established the spatiotemporal profile of intracellular calcium signals in epithelial prostate cancer cells. This spatiotemporal profile is determined by the flux of calcium ions across several biological membranes (e.g., endoplasmic reticulum or mitochondrial membranes), as well as by the diffusion mobility of Ca^{2+} and Ca^{2+} buffers in the cell (the so-called "buffered diffusion problem") (39).

As the cytosol may have heterogeneous Ca^{2+} buffering properties and intracellular membrane localization,

probably constituting a highly differentiated medium for spatial and temporal Ca^{2+} signals, it was essential to assess this property in a spatially resolved manner. Therefore, the different calcium signaling kinetics measured by patch-clamp and Ca^{2+} imaging techniques may be explained by the spatiotemporal properties of Ca^{2+} diffusion in the cytosol of prostate epithelial cells. Indeed, the channels revealing the agonist-activated cationic current in LNCaP cells may represent only a first step in the signal transduction pathway leading to $[Ca^{2+}]_i$ increase and the subsequent stimulation of cell proliferation. Further studies using different imaging techniques and dyes are required in order to understand this problem.

Our results demonstrate that Phe and OAG activate nearly identical cationic membrane currents in LNCaP cells. This therefore suggests that they may be transferred through the same population of ion channels. Indeed, both Phe- and DAG analogue–evoked currents shared the same electrophysiological properties (voltage dependence, preferential permeation of Ca^{2+} and Cs^{+} compared with Na^{+}, current density, and reversal potential) and pharmacological properties (sensitivity to 2-APB and SK&F 96365). Moreover, these channels seem to be insensitive to PKC, as PKC inhibitors did not interfere with the ability of OAG to induce Ca^{2+} entry, suggesting direct OAG gating. The strongest argument that both agonists target the same channel is the fact that neither of them was able to elicit additional current when applied during a maximal agonist-induced response. This would imply not only a common origin for the channels, but also that, at least under our experimental conditions, the α1-AR agonist Phe activates only those channels directly gated by DAG.

Our RT-PCR analysis of primary hPCE cells from prostate biopsies and LNCaP cells showed the presence of specific mRNA's for three TRP channels (TRPC1, TRPC3, and TRPC6) that may be implicated in both direct DAG gating and α1-AR signaling (16, 27–30). It is important to note that OAG induces exactly the same oscillatory $[Ca^{2+}]_i$ response in LNCaP cells as the α1-AR agonist Phe does in primary hPCE cells. As OAG is apparently capable of activating only store-independent Ca^{2+} entry, this strongly suggests that α1-AR–stimulated signaling in primary hPCE cells is preferentially coupled to store-independent TRP channels, whereas the major role in this signaling in LNCaP cells is played by store-operated TRP channels. Considering also that, according to our data, the TRPC1A splice variant and (to a lesser extent) TRPC3 may be DAG-gated channels common to both cell types (remember that primary hPCE cells express TRPC1A and TRPC6 strongly and TRPC3 weakly, whereas LNCaP cells express TRPC1A and TRPC3), a homo- or heterotetrameric assembly of these TRPs probably forms the endogenous DAG-gated cationic channel in prostate cancer epithelial cells.

Clinical implications. Targeting cell proliferation and apoptosis in an attempt to control prostate growth emerges as a potentially powerful therapeutic approach for the effective treatment of prostate cancer (40, 41).

Although α1-ARs are abundantly expressed in the prostate and the expression of some TRPs increases considerably during the progression to prostate cancer (42–44), no functional link between α1-ARs and TRPs has been firmly established, nor has their role in prostate cancer cell proliferation been elucidated. At the same time, all members of the signaling cascade from α1-ARs to the TRP channel may potentially serve as targets for therapeutic interventions aimed at cell proliferation. In this study, we establish a direct link between α1A-AR stimulation, the activation of TRP-mediated Ca^{2+} entry, and the proliferation of hPCE cells. Furthermore, we demonstrate that urospecific α1A antagonists such as prazosin and WB4101, as well as SK&F 96365, a known inhibitor of endogenous plasmalemmal cationic and TRP channels, suppress α1A-AR–induced cell proliferation. All together, our findings strongly indicate that the blockade of the α1A-AR–stimulated intracellular signaling pathway, not only at the receptor level, but also at the level of the affected channel, might be used for the treatment of prostate cancer. Effective testing of this possibility must await the development of potent and isoform-specific inhibitors of TRP channels.

Acknowledgments

We thank P. Delcourt and G. Lepage for their excellent technical assistance. This work was supported by grants from INSERM, the Ministère de l'Education Nationale, the Ligue Nationale Contre le Cancer, the Association pour la Recherche Contre le Cancer, and INTAS-99-01248. Y. Shuba was supported by INSERM and the Ministère de l'Education Nationale.

1. Woolf, S.H. 1995. Screening for prostate cancer with prostate-specific antigen. An examination of the evidence. *N. Engl. J. Med.* **333**:1401–1405.
2. Isaacs, J.T. 1994. Role of androgens in prostatic cancer. *Vitam. Horm.* **49**:433–502.
3. Isaacs, J.T., et al. 1992. Androgen regulation of programmed death of normal and malignant prostatic cells. *J. Androl.* **13**:457–464.
4. Caine, M. 1990. Alpha-adrenergic blockers for the treatment of benign prostatic hyperplasia. *Urol. Clin. North Am.* **17**:641–649.
5. Kyprianou, N., and Benning, C.M. 2000. Suppression of human prostate cancer cell growth by alpha1-adrenoceptor antagonists doxazosin and terazosin via induction of apoptosis. *Cancer Res.* **60**:4550–4555.
6. Benning, C.M., and Kyprianou, N. 2002. Quinazoline-derived alpha1-adrenoceptor antagonists induce prostate cancer cell apoptosis via an alpha1-adrenoceptor-independent action. *Cancer Res.* **62**:597–602.
7. Price, D.T., et al. 1993. Identification, quantification, and localization of mRNA for three distinct alpha 1 adrenergic receptor subtypes in human prostate. *J. Urol.* **150**:546–551.
8. Takeda, M., et al. 1999. alpha1- and alpha2-adrenoceptors in BPH. *Eur. Urol.* **36**(Suppl. 1):31–34.
9. Walden, P.D., Gerardi, C., and Lepor, H. 1999. Localization and expression of the alpha1A-1, alpha1B and alpha1D-adrenoceptors in hyperplastic and non-hyperplastic human prostate. *J. Urol.* **161**:635–640.
10. Fukasawa, R., et al. 1998. The alpha1L-adrenoceptor subtype in the lower urinary tract: a comparison of human urethra and prostate. *Br. J. Urol.* **82**:733–737.
11. Chapple, C.R., et al. 1994. Alpha 1-adrenoceptor subtypes in the human prostate. *Br. J. Urol.* **74**:585–589.
12. Marshall, I., Burt, R.P., and Chapple, C.R. 1999. Signal transduction pathways associated with alpha1-adrenoceptor subtypes in cells and tissues including human prostate. *Eur. Urol.* **36**(Suppl. 1):42–47.
13. Minneman, K.P. 1988. Alpha 1-adrenergic receptor subtypes, inositol phosphates, and sources of cell Ca2+. *Pharmacol. Rev.* **40**:87–119.

14. Kotlikoff, M.I., Herrera, G., and Nelson, M.T. 1999. Calcium permeant ion channels in smooth muscle. *Rev. Physiol. Biochem. Pharmacol.* **134**:147–199.
15. Clapham, D.E., Runnels, L.W., and Strubing, C. 2001. The TRP ion channel family. *Nat. Rev. Neurosci.* **2**:387–396.
16. Inoue, R., et al. 2001. The transient receptor potential protein homologue TRP6 is the essential component of vascular alpha(1)-adrenoceptor-activated Ca(2+)- permeable cation channel. *Circ. Res.* **88**:325–332.
17. Golovina, V.A., et al. 2001. Upregulated TRP and enhanced capacitative Ca(2+) entry in human pulmonary artery myocytes during proliferation. *Am. J. Physiol. Heart Circ. Physiol.* **280**:H746–H755.
18. Berridge, M.J. 1995. Calcium signalling and cell proliferation. *Bioessays.* **17**:491–500.
19. Grynkiewicz, G., Poenie, M., and Tsien, R.Y. 1985. A new generation of Ca2+ indicators with greatly improved fluorescence properties. *J. Biol. Chem.* **260**:3440–3450.
20. Skryma, R., et al. 2000. Store depletion and store-operated Ca2+ current in human prostate cancer LNCaP cells: involvement in apoptosis. *J. Physiol.* **527**:71–83.
21. Skryma, R.N., et al. 1997. Potassium conductance in the androgen-sensitive prostate cancer cell line, LNCaP: involvement in cell proliferation. *Prostate.* **33**:112–122.
22. Vanden Abeele, F., et al. 2002. Bcl-2-dependent modulation of Ca2+ homeostasis and store-operated channels in prostate cancer cells. *Cancer Cell.* **1**:169–179.
23. Watanabe, H., et al. 2002. Activation of TRPV4 channels (hVRL-2/mTRP12) by phorbol derivatives. *J. Biol. Chem.* **277**:13569–13577.
24. Roudbaraki, M., et al. 1999. Target cells of gamma3-melanocyte-stimulating hormone detected through intracellular Ca2+ responses in immature rat pituitary constitute a fraction of all main pituitary cell types, but mostly express multiple hormone phenotypes at the messenger ribonucleic acid level. Refractoriness to melanocortin-3 receptor blockade in the lacto-somatotroph lineage. *Endocrinology.* **140**:4874–4885.
25. Braun, F.J., Broad, L.M., Armstrong, D.L., and Putney, J.W., Jr. 2001. Stable activation of single Ca2+ release-activated Ca2+ channels in divalent cation-free solutions. *J. Biol. Chem.* **276**:1063–1070.
26. Diver, J.M., Sage, S.O., and Rosado, J.A. 2001. The inositol trisphosphate receptor antagonist 2-aminoethoxydiphenylborate (2-APB) blocks Ca2+ entry channels in human platelets: cautions for its use in studying Ca2+ influx. *Cell Calcium.* **30**:323–329.
27. Lintschinger, B., et al. 2000. Coassembly of Trp1 and Trp3 proteins generates diacylglycerol- and Ca2+- sensitive cation channels. *J. Biol. Chem.* **275**:27799–27805.
28. Zhu, X., Jiang, M., and Birnbaumer, L. 1998. Receptor-activated Ca2+ influx via human Trp3 stably expressed in human embryonic kidney (HEK)293 cells. Evidence for a non-capacitative Ca2+ entry. *J. Biol. Chem.* **273**:133–142.
29. Hofmann, T., et al. 1999. Direct activation of human TRPC6 and TRPC3 channels by diacylglycerol. *Nature.* **397**:259–263.
30. Tesfai, Y., Brereton, H.M., and Barritt, G.J. 2001. A diacylglycerol-activated Ca2+ channel in PC12 cells (an adrenal chromaffin cell line) correlates with expression of the TRP-6 (transient receptor potential) protein. *Biochem. J.* **358**:717–726.
31. Okada, T., et al. 1999. Molecular and functional characterization of a novel mouse transient receptor potential protein homologue TRP7. Ca(2+)-permeable cation channel that is constitutively activated and enhanced by stimulation of G protein-coupled receptor. *J. Biol. Chem.* **274**:27359–27370.
32. Smith, R.J., et al. 1990. Receptor-coupled signal transduction in human polymorphonuclear neutrophils: effects of a novel inhibitor of phospholipase C–dependent processes on cell responsiveness. *J. Pharmacol. Exp. Ther.* **253**:688–697.
33. Berven, L.A., and Barritt, G.J. 1995. Evidence obtained using single hepatocytes for inhibition by the phospholipase C inhibitor U73122 of store-operated Ca2+ inflow. *Biochem. Pharmacol.* **49**:1373–1379.
34. Mimura, Y., et al. 1995. Activation by alpha 1-adrenergic agonists of the progression phase in the proliferation of primary cultures of smooth muscle cells in mouse and rat aorta. *Biol. Pharm. Bull.* **18**:1373–1376.
35. Noveral, J.P., and Grunstein, M.M. 1994. Adrenergic receptor-mediated regulation of cultured rabbit airway smooth muscle cell proliferation. *Am. J. Physiol.* **267**:L291–L299.
36. Gao, B.B., Lei, B.L., Zhang, Y.Y., and Han, Q.D. 2000. Cell proliferation and Ca(2+)-calmodulin dependent protein kinase activation mediated by alpha 1A- and alpha 1B-adrenergic receptor in HEK293 cells. *Acta Pharmacol. Sin.* **21**:55–59.
37. McVary, K.T., McKenna, K.E., and Lee, C. 1998. Prostate innervation. *Prostate. Suppl.* **8**:2–13.
38. Rybalchenko, V., et al. 2001. Verapamil inhibits proliferation of LNCaP human prostate cancer cells influencing K+ channel gating. *Mol. Pharmacol.* **59**:1376–1387.
39. Naraghi, M., Muller, T.H., Neher, E. 1998. Two-dimensional determination of the cellular Ca2+ binding in bovine chromaffin cells. *Biophys. J.* **75**:1635–1647.
40. Plonowski, A., et al. 2002. Inhibition of in vivo proliferation of MDA-PCa-2b human prostate cancer by a targeted cytotoxic analog of luteinizing hormone-releasing hormone AN-207. *Cancer Lett.* **176**:57–63.
41. Crescioli, C., et al. 2002. Vitamin D3 analogue inhibits keratinocyte growth factor signaling and induces apoptosis in human prostate cancer cells. *Prostate.* **50**:15–26.
42. Peng, J.B., et al. 2001. CaT1 expression correlates with tumor grade in prostate cancer. *Biochem. Biophys. Res. Commun.* **282**:729–734.
43. Wissenbach, U., et al. 2001. Expression of cat-like, a novel calcium-selective channel, correlates with the malignancy of prostate cancer. *J. Biol. Chem.* **276**:19461–19468.
44. Tsavaler, L., Shapero, M.H., Morkowski, S., and Laus, R. 2001. Trp-p8, a novel prostate-specific gene, is up-regulated in prostate cancer and other malignancies and shares high homology with transient receptor potential calcium channel proteins. *Cancer Res.* **61**:3760–3769.